Quantum Transport Simulation of Bilayer pseudoSpin Field-Effect Transistor (BiSFET) with Tight-Binding Hartree-Fock Model

Xuehao Mou, Leonard F. Register and Sanjay K. Banerjee
Microelectronics Research Center, The University of Texas at Austin
10100 Burnet Road Building 160, Austin, Texas 78758, United States, Email: xmou@utexas.edu

***Abstract*—A simulation tool for modeling superfluid quantum transport in the proposed Bilayer Psuedo-spin Field Effect Transistor (BiSFET) and related systems is described and demonstrated. An interlayer Fock exchange interaction is incorporated into a π-orbital based atomistic tight-binding model of transport in two graphene layers separated by a tunnel barrier. Simulation results support and extend expectations based on bulk analysis such as superfluid condensate formation, enhanced interlayer tunneling and the sub-thermal voltage (sub-k_BT/q) switching. Extension of this method to other quasi-two dimensional material systems should be possible as well.**

Keywords—graphene; BiSFET; superfluid condensate;Fock exchange; atomistic tight binding; quantum transport

I. INTRODUCTION

The Bilayer pseudoSpin Field-Effect Transistor (BiSFET) is a novel "beyond CMOS device" concept based on the interlayer, electron-hole exciton condensates in two graphene layers [1]. It has been proposed that superfluid exciton condensates between n-type and p-type graphene layers separated by a tunnel dielectric, supported by interlayer many-body exchange interactions, could survive up to room temperature due to a synergy of graphene properties [2,3]. Such condensate formation, in turn, could provide novel transport effects such as enhanced interlayer tunneling and near perfect "Coulomb drag" [4-6]. The interlayer tunneling, however, can only be enhanced up to a "critical current" I_c and corresponding interlayer "critical voltage" V_c, much like in Josephson junctions and for similar reasons [5-8]. In principle, V_c can be lower than the thermal voltage k_BT/q, which is approximately 26 mV at T = 300 K. Consequently, it is possible to envision ultra-low voltage switching devices based on this effect, e.g., the BiSFET. Switching energies of tens of zepto Joules (~ 10^{-20} J) could be possible for the BiSFET with a (clocked) supply voltage ~ 25 mV [1], orders of magnitude less switching energy than "end-of-roadmap" CMOS.

The goal of this work is to allow first-principle simulation of basic transport behavior that might occur in the presence of such a condensate, although not to judge the precise conditions under which a condensate might be formed as in [3]. Here we describe a π-orbital-based atomistic tight-binding quantum transport simulator including a non-local interlayer Fock exchange interaction that allows simulation of the predicted novel transport effects. Illustrative simulations include the demonstration of a sub-k_BT/q value of V_c.

II. SIMULATED DEVICE STRUCTURE

We consider a four-terminal configuration for generality as Fig. 1. (The BiSFET requires only two contacts, e.g., top-left (T1) and bottom left (B1).) Two crystallographically aligned graphene layers are coupled within a region of effective dielectric ε = 2.2 including perhaps partial vacuums in the vicinity of the condensate region, above or below [3]. In the proposed BiSFET structure, the carrier concentrations would be controlled independently via two gate electrodes. In these simulations, the two layers are simply presumed to be gated to electrostatic potentials of $V_T = -V_B = 0.25$ V, corresponding to $n = p \approx 6\times10^{12}/\text{cm}^2$ in equilibrium with $E_F = 0$ eV. The exchange interaction is limited to the "interaction region"—starting with Unit Cell 1 and ending with Unit Cell N in Fig. 1—of length L in these simulations. Physically, the boundaries of the interaction region could be defined (less abruptly) by variations in the carrier densities, dielectric constants and/or layer separation. The voltages in the four semi-infinite leads, V_i, can be biased independently. The graphene layers are taken

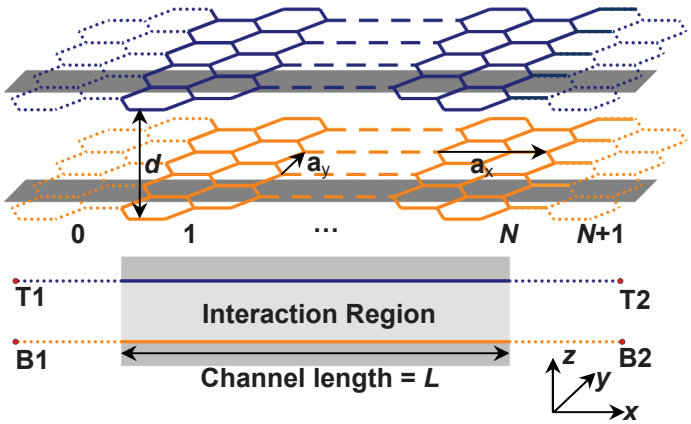

Fig. 1. Simulated device structure. Solid lines in hexagonal grid indicate interaction region (channel) and dotted lines indicate the semi-infinite leads. The shaded stripe corresponds to unit cell in the y dimension. Along the x-dimension, the unit cells are labeled as 1, 2… N within the interaction/channel region from left to right. The two gate electrodes above and below the interaction region are omitted here.

978-1-4673-5736-4/13/$31.00 ©2013 IEEE

to be infinitely wide (*y*-dimension). In all simulations, the interlayer spacing d = 1 nm and the temperature T = 300 K.

III. Basic Formalism

A. Tight-binding Schrödinger's Equation with Fock Exchange

The tight-binding Hartree-Fock Schrödinger's equation in the bottom (B) layer is

$$H_{\mathrm{TB}}\varphi_\beta(\mathbf{r}_\mathrm{B}) - qV_\mathrm{B}\varphi_\beta(\mathbf{r}_\mathrm{B}) + \sum_{\mathbf{R}_\mathrm{T}} V_{\mathrm{Fock}}(\mathbf{r}_\mathrm{B},\mathbf{R}_\mathrm{T})\varphi_\beta(\mathbf{R}_\mathrm{T}) = E_\beta\varphi_\beta(\mathbf{r}_\mathrm{B}) \quad (1)$$

and *vice versa* for the top (T) layer, where: H_{TB} describes the nearest neighbor intra-layer and bare/single-particle interlayer coupling; $V_{\mathrm{B(T)}}$ is the electrostatic potential; β is the combined state index indicating injecting lead α, energy band γ, energy E, transvers crystal momentum k_y, and (real) spin s; **r** denotes atom locations within a specific row of atoms along the length of the device (shaded gray regions in the hexagonal lattices of Fig. 1); and **R** denotes atom locations throughout the graphene layers. The interlayer Fock interaction is,

$$V_{\mathrm{Fock}}(\mathbf{r}_\mathrm{B},\mathbf{R}_\mathrm{T}) = -\frac{q^2}{4\pi\varepsilon|\mathbf{r}_\mathrm{B}-\mathbf{R}_\mathrm{T}|}\sum_\beta f_\beta\varphi_\beta(\mathbf{r}_\mathrm{B})\varphi_\beta^*(\mathbf{R}_\mathrm{T}) \quad (2)$$

where f_β is the Fermi occupation probability for state β as defined by the Fermi levels, $E_{\mathrm{F,i}} = -qV_\mathrm{i}$, and temperature. Given the periodicity in the transverse (*y*) direction, Eqs. (1) and (2) can be rewritten as

$$H_{\mathrm{TB}}\varphi_\beta(\mathbf{r}_\mathrm{B}) - qV_\mathrm{B}\varphi_\beta(\mathbf{r}_\mathrm{B}) + \sum_{\mathbf{r}_\mathrm{T}} A_{\mathrm{Fock},\omega_\mathrm{y}}(\mathbf{r}_\mathrm{B},\mathbf{r}_\mathrm{T})\varphi_\beta(\mathbf{r}_\mathrm{T}) = E_\beta\varphi_\beta(\mathbf{r}_\mathrm{B}) \quad (3)$$

and

$$A_{\mathrm{Fock},\omega_\mathrm{y}}(\mathbf{r}_\mathrm{B},\mathbf{r}_\mathrm{T}) = \sum_n V_{\mathrm{Fock}}(\mathbf{r}_\mathrm{B},\mathbf{r}_\mathrm{T}+n\mathbf{a}_\mathrm{y})e^{in\omega_\mathrm{y}} \quad (4)$$

respectively, where $\omega_\mathrm{y} = k_\mathrm{y}a_\mathrm{y}$ is the phase difference between adjacent primitive cells in the *y* direction, and n is an integer.

B. Boundary Conditions

In matrix notation, we may write the transport problem as

$$[E\mathbf{I} - \mathbf{H} - \mathbf{\Sigma}]\boldsymbol{\varphi} = \mathbf{S} \quad (5)$$

where: **H** is the Hamiltonia square matrix; **φ** is the wave-function column matrix which spans the entire simulation region; **S** is the source term, and has nonzero components only at the simulation region boundaries; **Σ** is the self-energy required to provide perfect boundary absorption of outgoing waves. (Eq. (5) is equivalent to the the non-equlibrium Greens Function calculation $\boldsymbol{\varphi}_\beta = \mathbf{G}\mathbf{S}_\beta$ where $\mathbf{G} = [E_\beta\mathbf{I} - \mathbf{H} - \mathbf{\Sigma}]^{-1}$, except that we do not need the full Green's function **G**.)

H can be subdivided into 8×8 submatrices $\mathbf{H}_{\mathrm{j,l}}$ for coupling within (j=l) and between (j≠l) the eight-atom unit cells along the simulation region. Similarly, $\boldsymbol{\varphi}_\beta$ can be subdivided into 1×8 vectors spanning each unit cell $\boldsymbol{\varphi}_{\beta,\mathrm{m}}$. Thinking of the boundary values of $\boldsymbol{\varphi}_\beta$ as just the sum of reflection (r) and—in general, nonzero in only leads—incident (i) waves, $\boldsymbol{\varphi}_\beta = \boldsymbol{\varphi}_{\beta,\mathrm{i}} + \boldsymbol{\varphi}_{\beta,\mathrm{r}}$, we may write for the left simulation region boundary for specificity:

$$\mathbf{H}_{10}(\boldsymbol{\varphi}_{\beta,\mathrm{i},0} + \boldsymbol{\varphi}_{\beta,\mathrm{r},0}) + \mathbf{H}_{11}\boldsymbol{\varphi}_{\beta,1} + \mathbf{H}_{12}\boldsymbol{\varphi}_{\beta,2} = E_\beta\boldsymbol{\varphi}_{\beta,1} \quad (6)$$

Moreover, $\boldsymbol{\varphi}_{\beta,\mathrm{r},0}$ may be determined from $\boldsymbol{\varphi}_{\beta,1}$ and $\boldsymbol{\varphi}_{\beta,\mathrm{i},0}$ as,

$$\boldsymbol{\varphi}_{\beta,\mathrm{r},0} = \mathbf{P}_{\mathrm{r},10}\boldsymbol{\varphi}_{\beta,\mathrm{r},1} = \mathbf{P}_{\mathrm{r},10}(\boldsymbol{\varphi}_{\beta,1} - \boldsymbol{\varphi}_{\beta,\mathrm{i},1}) = \mathbf{P}_{\mathrm{r},10}(\boldsymbol{\varphi}_{\beta,1} - \mathbf{P}_{\mathrm{i},01}\boldsymbol{\varphi}_{\beta,\mathrm{i},0}) \quad (7)$$

where the 8×8 matrix $\mathbf{P}_{\mathrm{i},01}$ ($\mathbf{P}_{\mathrm{r},10}$) propagates the incident (reflection) wave-function one unit cell across the simulation region boundary. If, e.g., $\boldsymbol{\varphi}_{\mathrm{i},0}$ is an incident Bloch function in one left-side lead with *x*-directed crystal momentum $\hbar k_\mathrm{x}$, then $\mathbf{P}_{\mathrm{i},01}\boldsymbol{\varphi}_{\mathrm{i},0} = e^{ik_\mathrm{x}a_\mathrm{x}}\boldsymbol{\varphi}_{\mathrm{i},0}$. Substituing (7) back into (6) gives,

$$(\mathbf{H}_{11} - E_\beta\mathbf{I} + \mathbf{H}_{10}\mathbf{P}_{\mathrm{r},10})\boldsymbol{\varphi}_{\beta,1} + \mathbf{H}_{12}\boldsymbol{\varphi}_{\beta,2} = \mathbf{H}_{10}(\mathbf{P}_{\mathrm{r},10}\mathbf{P}_{\mathrm{i},01} - \mathbf{I})\boldsymbol{\varphi}_{\beta,\mathrm{i},0} \quad (8)$$

allowing the self-energy to be identified as $\mathbf{\Sigma}_{1,1} = -\mathbf{H}_{10}\mathbf{P}_{\mathrm{r},10}$ and the source as $\mathbf{S}_1 = \mathbf{H}_{1,0}(\mathbf{P}_{\mathrm{r},10}\mathbf{P}_{\mathrm{i},01} - \mathbf{I})\boldsymbol{\varphi}_{\mathrm{i},0}$. Similary $\mathbf{\Sigma}_{\mathrm{N,N}} = -\mathbf{H}_{\mathrm{N,N+1}}\mathbf{P}_{\mathrm{r,N,N+1}}$ and $\mathbf{S}_\mathrm{N} = \mathbf{H}_{\mathrm{N,N+1}}(\mathbf{P}_{\mathrm{r,N,N+1}}\mathbf{P}_{\mathrm{i,N+1,N}} - \mathbf{I})\varphi_{\mathrm{i,N+1}}$. All other matrix components $\mathbf{\Sigma}_{\mathrm{j,l}}$ and $\mathbf{S}_\mathrm{m}$ are zero.

IV. Numerical Approach

Superfluid condensate formation is characterized by a self-consistent exchange interaction and gap formation; the stronger the coupling between layers, the greater the coherence, the greater the exchange interaction and associated band gap [2,8]. We employ an iterative method to solve this self-consistent quantum transport-Fock exchange problem, conceptually much as used to obtain self-consistent solutions of the quantum transport-Poisson equations, except that the Fock interaction is highly non-local in position. This non-locality increases the computational challenge substantially and parallel computing is used to speed up calculations.

However, for each iteration, the transport problem can be subdivided by energy and k_y, and the Fock interaction can be analyzed as non-local only in position along the channel (within the shade gray regions of Fig. 1 again) consistent with Eq. (4). Moreover, Eq. (4) can be rewritten as,

$$A_{\mathrm{Fock},\omega_\mathrm{y}}(\mathbf{r}_\mathrm{B},\mathbf{r}_\mathrm{T}) = \sum_{\omega_\mathrm{y}'} C(\mathbf{r}_\mathrm{B},\mathbf{r}_\mathrm{T};\omega_\mathrm{y},\omega_\mathrm{y}') \sum_{\alpha',\gamma',E',s'} f_{\beta'}\varphi_{\beta'}(\mathbf{r}_\mathrm{B})\varphi_{\beta'}^*(\mathbf{r}_\mathrm{T}) \quad (9)$$

where

$$C(\mathbf{r}_\mathrm{B},\mathbf{r}_\mathrm{T};\omega_\mathrm{y},\omega_\mathrm{y}') = -\sum_n \frac{q^2}{4\pi\varepsilon|\mathbf{r}_\mathrm{B}-\mathbf{r}_\mathrm{T}-n\mathbf{a}_\mathrm{y}|}e^{in(\omega_\mathrm{y}-\omega_\mathrm{y}')} \quad (10)$$

depends only on $\mathbf{r}_\mathrm{B} - \mathbf{r}_\mathrm{T}$ and $\omega_\mathrm{y} - \omega_\mathrm{y}$ and can be pre-calculated. (Also, $C(\mathbf{r}_\mathrm{B},\mathbf{r}_\mathrm{T};\omega_\mathrm{y},\omega_\mathrm{y}') = C^*(\mathbf{r}_\mathrm{T},\mathbf{r}_\mathrm{B};\omega_\mathrm{y},\omega_\mathrm{y}') = C^*(\mathbf{r}_\mathrm{B},\mathbf{r}_\mathrm{T};\omega_\mathrm{y}',\omega_\mathrm{y})$ allowing memory space to be saved as needed). For a given iteration, differing CPUs are used to calculate the differing wave-functions $\boldsymbol{\varphi}_\beta$ via Eq. 5, and then to calculate the differing new Fock contributions $A_{\mathrm{Fock},\omega_\mathrm{y}}(\mathbf{r}_\mathrm{B},\mathbf{r}_\mathrm{T})$ via Eq. (9), which is repeated with the new Fock exchange interaction until convergence—or lack thereof as to be discussed below—is established.

The condensate is created by states within the vicinity of the associated band gaps [7]. Here we consider an injected energy range of ± 1.5 eV about the equilibrium Fermi level, which has been proved more than enough. Also, the range of the Fock interaction is generally < 5 nm, allowing $\mathbf{r}_\mathrm{B} - \mathbf{r}_\mathrm{T}$ and n to be restricted. Finally, because different (real) spins do not interact, we simulated only one, and then doubled properties such as local density of states and current to include the other.

V. Results and Discussion

A. Condensate Formation

As noted earlier, condensate formation is characterized by a self-consistently enhanced exchange interaction and formation of an associated band gap [2]. To monitor the

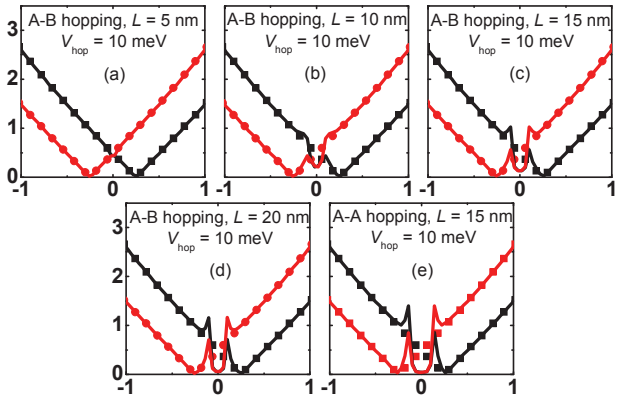

Fig. 2. The local density of states in the center of the channel for V_{hop} = 10 meV with varying channel length. Red (gray in the black & white printouts) curves for top band and black curves for bottom band. Unperturbed LDOS is plotted in scattered points.

condensate formation, we calculated the local density of states (LDOS). Fig. 2 shows the LDOS as a function of energy at the center of interaction/channel region for varying channel lengths and interlayer bare coupling patterns, along with the exchange-free result for comparison. A substantial, if still incompletely formed, band gap has formed in the center of the interaction region when L reaches 15 nm, as seen in the substantial drop in the LDOS over an energy range of approximately 200 meV around the Fermi level E_F = 0 eV. The expulsion of the LDOS from the band gap is also evidenced by the spikes at the nominal "band edges". Though incompletely formed, this ~ 200 meV gap is consistent with our bulk calculations with the same system parameters [7,8]. To form an effectively complete band gap, one would need quite long channels, which would be undesirable for device design as well as computationally expensive. As it turns out, the partial condensate formation for L = 15 nm is sufficient to exhibit the transport properties of interest here, and L = 15 nm is used henceforth.

We also considered two representative forms of interlayer coupling, A-A hopping between only A sublattices on either layer, and A-B hopping. (The latter is Bernal-like but much weaker. However, the coupling is through a dielectric and not intrinsically Bernal-like.) Because A-B hopping is nearly orthogonal to the natural coupling pattern of the condensate, it is expected to be less effective at enhancing interlayer tunneling current than the A-A pattern [7, 8], as suggested by the differences in partial band-gaps shown in Fig. 2 (c) and (e). We consider only A-A hopping, henceforth.

B. Enhanced Interlayer Transmission Probabilities

We then calculated the average intra- and inter-layer transmission coefficients averaged across all incident states β of the same lead at energy E, $T(E)$, under *equilibrium* conditions, with an interlayer bare hopping energy of V_{hop} = 1 meV, with and without the exchange interaction and associated condensate formation. The results for states incident in leads T1 and B1 (see Fig. 1 again) are plotted in Fig. 3. (Note that detailed balance is satisfied in all cases, but the *averaged* transmission probabilities T1→B1 and B1→T1 need not be the same as a function of energy as there can be more carriers incident from one lead or the other at the same

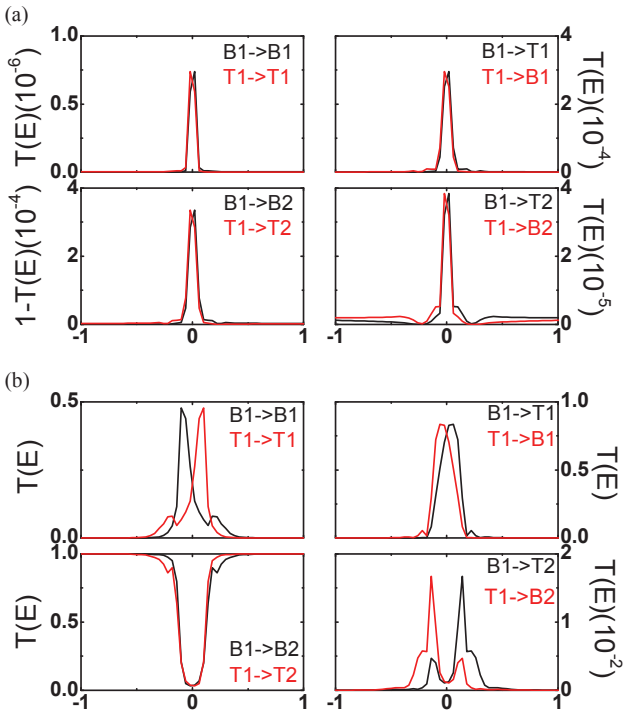

Fig. 3. Averaged transmission coefficient $T(E)$ for electrons incident in leads B1 and T1 under equilibrium conditions with V_{hop} = 1 meV. Results absent the exchange interaction and associated condensate are plotted in (a) for reference, and with the exchange interaction and condensate in (b).

energy. However, upon inversion about E = 0 eV, the $T(E)$ overlap again.) The interlayer transmission probabilities are greatly increased—over three orders of magnitude (top-right of Figs. 3(a) and (b))—in the presence of condensates. The peak interlayer transmission probability is around 80% (top-right of Fig. 3(b)) which occurs near the center of the gap, with the corresponding intra-layer transmission damped to almost zero (bottom-left of Fig. 3(b)). These results suggest that in the low-voltage Laudauer-Büttiker limit, the top and bottom layers are nearly shorted together on the same ends by condensate formation, while opposite ends of the channel are strongly isolated.

C. Non-equilibrium Transport

We first discuss qualitatively expected behavior. To aid the discussion, we note that the "which-layer" degree of freedom can be referred to as the "pseudospin" analogous to real spin, where the condensates are viewed as coherent pseudospin states with a corresponding pseudospin phase. (This terminology is the origin of the BiSFET moniker.) Moreover, *although we do not make this assumption in our transport calculations*, we note that the pseudospin phase relation between layers is expected to be a roughly global function for this collective many-body state [7,8]. Analogous to current between two points/orbitals in any tight-binding calculation, current flow requires that the product of the interlayer pseudo-spin (condensate) and the interlayer coupling/hopping potential have an imaginary component. However, in the above global phase approximation, pseudospin phase is inherently opposite to the phase of the Fock exchange interaction between any two points (see Eq. (2)), so that the product is real and the exchange interaction alone cannot carry any interlayer current I_{il}. Instead, I_{il} depends on the imaginary

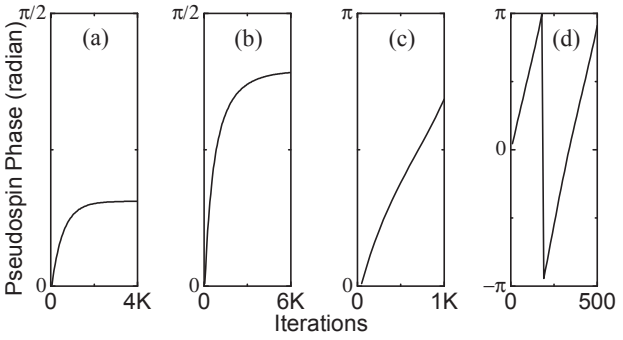

Fig. 4. Starting form equilibrium solutions, the pseudospin rotation (specifically between A atoms on opposite layers at the center of the interaction/channel region) are shown as a function of iteration number under the condition of: (a) V_{hop} = 0.5 meV and V_{il} = 5 mV, (b) V_{hop} = 0.5 meV and V_{il} = 10 mV, (c) V_{hop} = 0.5 meV and V_{il} = 20 mV, and (d) V_{hop} = 0.5 meV and V_{hop} = 100 mV from left to right respectively. (a) and (b) are consistent with stable DC behavior below a critical voltage; (c) and (d) are consistent with the collapse of DC behavior and unstable oscillatory behavior beyond a critical voltage. In particular, (c) illustrates that the critical voltage can be less than the thermal voltage $k_BT/q \approx 26$ mV in these 300 K simulations.

component of product of the pseudospin (the condensate) and the bare coupling. Therefore, for a given pseudospin magnitude (condensate strength) and real bare coupling, there should be a maximum DC value of I_{il}, the critical current I_c, that can flow between layers which is reached when the pseudospin phase reaches $\pm\pi/2$ radians [7,8]. That is, the interlayer voltage V_{il} can continue to increase beyond the associated critical voltage V_c, but the DC value of I_{il} cannot. Instead, beyond V_c, the pseudospin is expected to rotate in time, at a rate proportional to V_{il} (at about 250 GHz per meV) producing an oscillating interlayer current I_{il} even with fixed V_{il}. These expectations are analogous in both behavior and cause to the well-known DC and AC Josephson effects abruptly separated by a critical voltage.

To study the non-equilibrium transport properties here, we applied an interlayer voltage V_{il} to the left-end contacts between the layers such that $E_{F,T1} = -E_{F,B1} = -qV_{il}/2$ and $E_{F,T2} = E_{F,B2} = 0$ eV. The current and exchange interactions were calculated self-consistently. The electrostatic potential were held fixed to $V = \pm 0.25$ V, but we note that the carrier concentrations were only weakly perturbed for the $V_{il} \leq k_BT/q$ of importance here.

As shown in Fig. 4(a)-(c), the two predicted limiting behaviors are observed as a function of V_{il} for fixed V_{hop}. For (a) V_{hop} = 0.5 meV and V_{il} = 5 mV, and (b) V_{hop} = 0.5 meV, V_{il} = 10 mV, a stable-self-consistent solution is found with $I_{il} \approx 76$ and 152 μA/μm, respectively. In contrast, for V_{hop} = 0.5 meV and V_{il} = 20 meV, while pseudospin (condensate) remains strong throughout the iterative simulation procedure, no stable solution is found. Instead, the pseudospin continues to rotate with iteration. With V_{il} increased to 100 mV to produce faster (less computationally expensive) rotation with iteration, the never-ending pattern of phase rotation, suggestive of time-dependent oscillations, becomes more overt in Fig. 4(d). Critically, we note that for these simulations, a V_c less than 20 mV—approximately 11 mV based on the extrapolation of the sine of the pseudo-spin phase with V_{il} to unity (pseudospin phase to π/2)—illustrates the possibility of sub-k_BT/q critical voltages that underlie the proposed ultra-low-power BiSFET device concept. Indeed, there is nothing in these simulations which suggests that V_c could not be reduced arbitrarily with reduction in V_{hop} independent of temperature.

VI. Conclusion

We have described and demonstrated a simulation tool for modeling superfluid quantum transport in the proposed Bilayer psuedo-Spin Field Effect Transistor (BiSFET) and related systems. An interlayer Fock exchange interaction is incorporated into a π-orbital based atomistic tight-binding model of transport in two graphene layers separated by a tunnel barrier. Simulation results are consistent with previous bulk equilibrium-based predictions of superfluid condensate formation, associated enhanced interlayer tunneling and the sub-thermal voltage (sub-k_BT/q) critical voltages, and, thus, possible sub-k_BT/q switching, which collectively serve as the basis for the proposed BiSFET device concept for ultra-low-power switching.

The four-terminal device structure considered here, which has two more leads than the proposed BiSFET, also will allow investigation of other biasing conditions, such as the "drag-counterflow" biasing condition expected to produce near-perfect Coulomb drag between layers up to significantly higher voltages [5,6].

Finally, we note that the basic numerical method allows consideration of other tight-binding Hamiltonians and, thus, other quasi-two dimensional material systems.

Acknowledgment

This work was supported by the Semiconductor Research Corporation (SRC)'s Nanoelectronics Research Initiative (NRI). Supercomputing resources were provided by the Texas Advanced Computing Center (TACC).

References

[1] S. K. Banerjee, L. F. Register, E. Tutuc, D. Reddy and A. H. MacDonald, "Bilayer pseudospin field-effect transistor (BisFET): A proposed new logic device", *IEEE EDL*, vol. 30, no. 2, 2009

[2] H. Min, R. Bistritzer, J.-J. Su and A. H. MacDonald, "Room-temperature superfluidity in graphene bilayers", *Phys. Rev. B* 78, 121401 (R), 2008

[3] I. Sodemann, D. A. Pesin and A. H. MacDonald, "Interaction-enhanced coherence between two-dimensional Dirac layers", *Phys. Rev. B* 85, 195136, 2012

[4] L. Tiemann, W. Dietsche, M. Hauser and K. von Klitzing, "Critical tunneling currents in the regime of bilayer excitons", *New J. Phys.* 10, 045018, 2008

[5] J. –J. Su, A. H. MacDonald, "How to make a bilayer exciton condensate flow", *Nat. Phys.* 4, 799-802, 2008

[6] D. Nandi, A. D. K. Finck, J. P. Eisenstein, L. N. Pfeiffer and K. W. West, "Exciton condensation and perfect Coulomb drag, *Nature* 488, 481-484, 2012

[7] D. Basu, L. F. Register, D. Reddy, A. H. MacDonald and S. K. Banerjee, "Tight-binding study of electron-hole pair condensation in graphene bilayers: Gate-control and system-parameter dependence", *Phys. Rev. B*, 82, 075409, 2010

[8] D. Basu, L. F. Register, A. H. MacDonald and S. K. Banerjee, "Effect of interlayer bare tunneling on electron-hole coherence in graphene bilayers," *Physical Review B* 84, 0354489, 2011.